








# Spontaneous parametric down-conversion in bottom-up grown lithium niobate microcubes

NGOC MY HANH DUONG,<sup>1,4,5,\*</sup>  GRÉGOIRE SAERENS,<sup>1,4</sup>  FLAVIA TIMPU,<sup>1</sup> MARIA TERESA BUSCAGLIA,<sup>2</sup> VINCENZO BUSCAGLIA,<sup>2</sup> ANDREA MORANDI,<sup>1</sup> JOLANDA S. MÜLLER,<sup>1</sup> ANDREAS MAEDER,<sup>1</sup>  FABIAN KAUFMANN,<sup>1</sup> ALEXANDER S. SOLNTSEV,<sup>3</sup>  AND RACHEL GRANGE<sup>1,6</sup> 

<sup>1</sup>ETH Zurich, Optical Nanomaterial Group, Institute for Quantum Electronics, Department of Physics, 8093 Zurich, Switzerland

<sup>2</sup>Institute of Condensed Matter Chemistry and Technologies for Energy, National Research Council, Via de Marini 6, 16149 Genoa, Italy

<sup>3</sup>School of Mathematical and Physical Sciences, University of Technology Sydney, Ultimo, New South Wales, 2007, Australia

<sup>4</sup>These authors contributed equally to this work

<sup>5</sup>[nduoeng@phys.ethz.ch](mailto:nduoeng@phys.ethz.ch)

<sup>6</sup>[grange@phys.ethz.ch](mailto:grange@phys.ethz.ch)

\*[dnmyhanh@gmail.com](mailto:dnmyhanh@gmail.com)

**Abstract:** Nonclassical light sources are highly sought-after as they are an integral part of quantum communication and quantum computation devices. Typical sources use bulk nonlinear crystals that rely on stringent phase-matching conditions, limiting the operating wavelength and bandwidth. In this work, we demonstrate the generation of photon pairs from a free-standing lithium niobate microcube at the telecommunication wavelength of 1.56  $\mu\text{m}$  through the spontaneous parametric down-conversion process. The maximum photon pair generation rate obtained from a single microcube with the size of 3.6  $\mu\text{m}$  is 490 Hz, resulting in an efficiency of 20.6 GHz/Wm, which is three orders of magnitude larger than the efficiency of biphoton generation in bulk nonlinear crystals. The microcubes are synthesized through a solvothermal method, offering the possibility for scalable devices via bottom-up assembly on any substrates. Our work constitutes an important step forward in the realization of compact nonclassical light sources with a wide bandwidth for various quantum applications.

© 2022 Optica Publishing Group under the terms of the [Optica Open Access Publishing Agreement](#)

## 1. Introduction

A photon pair source is an important building block for applications in quantum communication, quantum networks, and quantum computation [1–4]. So far, spontaneous wave-mixing processes, including four-wave mixing [5,6], and three-wave mixing have been considered versatile techniques for the generation of nonlinear correlated photon pairs [1]. Between the two techniques, the three-wave mixing process or spontaneous parametric down-conversion (SPDC) [7], which exploits the second-order nonlinearity, can achieve higher conversion efficiency compared to its third-order counterpart in the same nonlinear material volume, except for the cases of nontrivial mode overlap [8]. SPDC is considered one of the most promising processes for the generation of photon pairs owing to its robust operation at room temperature, high photon pair rates, and ability to prepare entangled states in several degrees of freedom such as polarization [9,10], angular momentum [11], and frequency [12].

Alternative platforms for nonclassical light generation have been realized in optically active solid-state defects including fluorescent color centers [13,14], quantum dots (QDs) [15], and two-dimensional materials such as transition metal dichalcogenides (TMDCs) [16,17] and hexagonal

boron nitride [18,19]. These systems can be used to generate single photons, competing with heralded single-photon generation via spontaneous parametric nonlinear processes [20], and can also generate photon pairs, including entangled photon pairs [21]. However, QDs and the TMDCs only exhibit nonclassical photon emission that is suitable for quantum applications at cryogenic temperatures, which involves expensive and bulky cooling systems. All these sources also suffer from inhomogeneous distributions and spectral diffusion due to the charges in the solid-state host environment [22], thus making it difficult to generate two correlated photons from different emitters. Moreover, interfacing those atomic defects to photonic structures remains a non-trivial task due to the high refractive index of the host materials, which makes the extraction of photons challenging. Additionally, there is only a limited number of quantum light sources that can generate single photons at telecom wavelengths [23], which are used in conventional long-distance optical communication systems where the losses are the lowest. Therefore, the quest for an ideal photon pair source, which operates at room temperature and possesses high brightness, high heralding efficiency, and high indistinguishability is still ongoing. The efficiency of the SPDC process is improved for systems with satisfied phase-matching conditions. Conventionally, phase-matching conditions can be achieved by using birefringent crystals [10,24]. However, these sources offer relatively low photon pair rates and limited wavelength ranges due to the phase-matching constraints. Another approach is to use periodically poled waveguides with periodically inversed poled domains, which change the sign of quadratic nonlinear susceptibility [24–27]. This method can significantly improve the conversion efficiency of the SPDC process but still results in long devices with lengths of tens to hundreds of microns [28], which is challenging for complex and densely integrated photonics.

A promising emerging approach is miniaturized SPDC quantum light sources based on nonlinear materials. Recently, photon pair generation through SPDC has been realized in thin films at the micro- and nanoscale ranges in materials with large second-order nonlinear susceptibility such as lithium niobate (LN) [29,30], and gallium phosphide (GaP) [30]. These studies opened new possibilities for non-phase-matched SPDC, where the phase-matching restrictions no longer exist owing to the small interaction length. In this case, the conversion efficiency of the nonlinear process primarily depends on the large quadratic nonlinearity of the medium since the total interaction length is limited. Following the demonstrations of SPDC in nonlinear thin films, it has been theoretically shown that nonlinear material based nanoresonators supporting Mie-like resonances can be versatile sources of photon pairs due to the high refractive index and strong intrinsic nonlinearity of the material, combined with amplified vacuum fluctuations within the resonant structures, leading to a more efficient SPDC process [31]. Initial experiments have also been realized in AlGaAs nanoresonators [32], and LN metasurfaces [33]. Nevertheless, these approaches require careful modal matching [34], and sophisticated top-down fabrication techniques, which are significant scale-up challenges. This research direction towards miniaturized SPDC sources with relaxed phase-matching constraints has just started and may profit the scientific community with a scalable and integrable platform for the study of nonlinear phenomena at the microscale.

Here, we present a generation of photon pairs at the telecommunication wavelengths via the SPDC process from bottom-up grown LN microcubes with sizes ranging from 2 to 5  $\mu\text{m}$ . The conventional fabrication of single-crystalline LN thin films normally requires the Czochralski method [35], followed by ion slicing [36], titanium in-diffused [37], wafer bonding [36], and ion-beam-enhanced etching in combination with electron-beam lithography [38], or focus ion beam (FIB) milling [39] to obtain micro-or nanoresonators. These methods are cumbersome and involve several sophisticated steps, resulting in expensive LN devices. Contrary to these platforms [29,30,33], our structures are free-standing microcubes, obtained through a solvothermal process. This bottom-up synthesis approach does not only provide monocrystalline LN structures that can be deposited deterministically on any substrates but also enables scalability since it can be

combined with soft nanoimprint lithography to create metamaterial structures over a large surface area.

LN is the ideal material choice due to its extraordinary optical properties such as a wide transparent window ranging from 0.3-5.0  $\mu\text{m}$ , a low absorption coefficient, and especially a high second-order ( $\chi^{(2)}$ ) optical susceptibility. The generation of photon pairs through SPDC from LN microcubes opens the opportunity for integrable two-photon light sources at the microscale, which allows the miniaturization of functional quantum devices. Compared to QDs or defect-based photon sources, heralded single-photon sources based on SPDC occur at room temperature, eliminating the need for a cryogenic chamber, and thus reducing the cost of equipment. Compared to other nonlinear approaches, owing to the relaxation of longitudinal phase-matching, our system can produce photon pairs in a wide range of wavelengths [28,29], and enable the realization of metasurfaces [33] with the control of the phase front of the generated photon pairs for potential applications in free-space quantum communication, quantum computing, and quantum metrology.

## 2. Results and discussions

A LN powder consisting of microcubes with the size of 2-5  $\mu\text{m}$  (Fig. S1) was synthesized via a solvothermal process, starting from niobium pentoxide ( $\text{Nb}_2\text{O}_5$ ) and lithium hydroxide (LiOH) precursors (see Supplementary, section 1 for more details). The samples were prepared by spin coating the LN powder diluted in ethanol on a substrate with patterned reference markers. An example of a single LN microcube for SPDC process (Fig. 1(A)) is shown in the scanning electron microscope (SEM) image in Fig. 1(B). We measured only LN microcubes that are at least 20  $\mu\text{m}$  apart from each other on the substrate, as shown in Fig. 1(C), to ensure that only emission from a single cube is collected. The excitation laser is focused down to a spot of 8  $\mu\text{m}$  in diameter, which fully covers single cubes, and the generated photons were collected with a high numerical aperture (NA) objective (Fig. 1(B)).

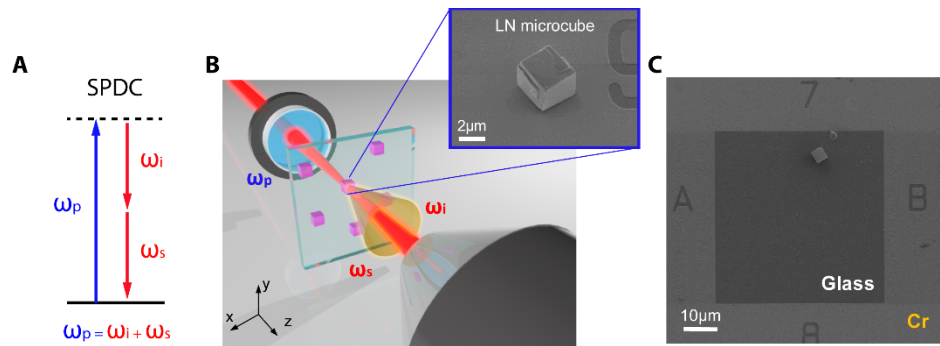


**Fig. 1.** (A) Diagram of the SPDC process. (B) Schematic of the transmission setup for LN microcube optical characterization. Inset: SEM image of an example of a typical microcube in this study. (C) SEM image of the sample showing a distribution of various LN microcubes on the substrate with markers. The brighter area around the 50  $\mu\text{m}$  dark square area is covered with Cr to enable electronic transport during SEM imaging.

To study the photon pair generation process, we performed the second-order auto-correlation measurements on a Hanbury-Brown-Twiss setup (see Supplementary, Fig. S2), using a continuous wave (CW) laser with a center wavelength of  $\sim 780$  nm to generate photons at  $\sim 1560$  nm via SPDC. Figure 2(A) is an SEM image of a microcube (cube 1) with a size of 3.0  $\mu\text{m}$ . As the LN cube is of rhombohedral structure, we can assume that the width, length, and height are almost equal [40]. The second-order autocorrelation function measurement on cube 1, acquired for 180 minutes at a pump power of 50 mW, demonstrated a correlation peak at the zero-delay time.

The coincidences-to-accidentals ratio (CAR) exceeds 2 ( $CAR = g^{(2)}(0) - 1 = 360$ ), indicating simultaneous arrival of the two photons (Fig. 2(B)).

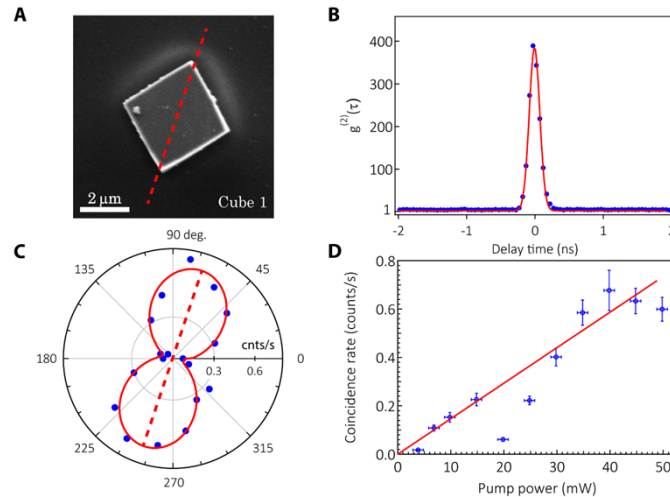


**Fig. 2.** SPDC characterizations of a single microcube. (A) SEM image of a single LN microcube with the optical axis (red dashed line) at  $\sim 70^\circ$  with respect to the zero-polar axis. (B) Autocorrelation function measurement on the cube in Fig. 1(B), demonstrating a correlation peak at zero-delay time. (C) Real biphoton rate from the cube as a function of pump polarization, and the data is fitted using  $\cos^2\theta$  function (solid red line). (D) Power dependence measurement demonstrated a linear dependence between the biphoton rate from the microcube (blue circle) upon the excitation with different fundamental pump powers, the red line is the linear fitting. Due to some fluctuation in the pump laser or the setup alignment, the measurement at 20 mW is lower than expected, though, we obtained the expected behavior that SPDC signal scales linearly with pump power in the low gain regime [41].

Figure 2(C) shows the polarization dependence of the photons emitted from cube 1 (blue circle) with respect to the polarization of the excitation laser. The polarization axis of the microcube is oriented along the diagonal of the rhombohedron, which is the projection of the c-axis, i.e., the spontaneous polarization vector of the LN crystal on the lateral face [40,42]. Specifically, the red dashed line in Fig. 2(A) indicates the direction of the polarization axis, yielding an angle of  $\sim 70^\circ$  relative to the horizontal line in the frame of the lab (see Supplementary, section 6 for more information of the measurements). The linear light polarization is defined clearly from a polarized beam splitter and its orientation is rotated with a half-wave plate. We took into account the rotation and changes happening to the horizontal component of polarization as it is reversed at each mirror. Due to the form of  $\chi^{(2)}$  susceptibility tensor of the material [42], the SPDC signal is maximal when the excitation laser is polarized along this axis of the cube (Fig. 2(C)).

Next, we performed the power dependence measurements to further characterize the system. The second-order autocorrelation function was obtained while changing the pump power from 4 to 50 mW (Fig. 2(D)). The measurement demonstrates a linear dependence between the biphoton rate and the pump power [41]. Specifically, we measured a photon emission rate of  $\sim 0.74$  Hz for cube 1. After correcting for the various transmission loss originating from the optical components (see Supplementary, section 3 for more details), the transmission corrected photon pair rate from cube 1 is  $160 \pm 24$  Hz, resulting in conversion efficiency of  $11.6 \pm 1.8$  GHz/Wm; this value was obtained by normalizing the transmission corrected biphoton rate with the volume of the structure and the intensity of the pump.

We estimated the two-photon generation rate from microcubes of different sizes by evaluating the efficiency of the inverse process of SPDC, namely sum-frequency generation (SFG), which has the same origin due to the quantum-classical correspondence principle [43,44]. The total photon pair generation rate across the area of the cube can then be calculated via the relation [44]:

$$\frac{1}{P_p} \frac{dN_{pair}}{dt} = 2\pi\eta^{SFG} \frac{\lambda_p^4}{\lambda_s^3 \lambda_i^3} \frac{c\Delta\lambda}{\lambda_s^2} \quad (1)$$

Here  $P_p$  represents the pump beam power,  $dN_{pair}/dt$  is the photon pair generation rate per unit signal frequency,  $\eta^{SFG} = P_{SFG}/P_s P_i$  is the sum-frequency conversion efficiency,  $\lambda_p$ ,  $\lambda_s$ , and  $\lambda_i$  are the pump, signal, and idler wavelengths, respectively. Considering only the degenerate SPDC process, we then derived the photon pair rate by applying the efficiency of another analogous and inverse process of SPDC, i.e., second-harmonic generation (SHG). In this specific case,  $\lambda_s = \lambda_i = \lambda_p/2$ , and Eq. (1) becomes:

$$\frac{1}{P_p} \frac{dN_{pair}}{dt} = 2\pi\eta^{SHG} 256 \frac{c\Delta\lambda}{\lambda_p^4} \quad (2)$$

with  $\eta^{SHG}$  being the efficiency of the SHG process, which can be analytically calculated for cubes with various sizes as described in the Ref. [45]. The results are plotted in Fig. 3(A), demonstrating a ten-fold increase in the biphoton rate upon increasing the size of the cubes from 1 to 4  $\mu\text{m}$ . The predicted value for biphoton rate from a LN microcube of 3  $\mu\text{m}$  is around 6000 Hz at the pump power of 50 mW, however, the experimental value for cube 1 is 40 times lower due to collection NA of 0.65, and defects in the crystalline structure.

To gain an insight into the emission of the biphotons, we performed a simulation using the Finite Element Method (FEM) (see Supplementary, section 4 for more details) for the SFG process and then predicted the polarization states and far-field emission pattern of the SPDC process, which is proportional to the SFG amplitude of the classical signal and idler photons. In particular, we exploited the non-collinear detection scheme limited within the angle  $\theta$  defined by the numerical aperture of the objective (NA = 0.65) to simulate the polarization states of generated photons. In this specific collection configuration, the generated photons are polarized in the x-y plane, hence, we explored the nonlinear process efficiency between x and y linear polarizations of signal and idler photons with x-polarization along the optical axis. Figure 3(B) presents the simulation results, showing the photon pairs generated from the microcube mostly share the same x-polarization due to the nonlinear susceptibility tensor.

We then predicted the radiation profiles of SPDC emission through SFG simulation. Specifically, we performed simulation using a model where the cube was sitting on a glass substrate and excited from the glass side or the air side (Supplementary, Fig. S4). Figure 3(C) demonstrates that biphotons are mainly generated forward or backward along the z-direction, collinear to the direction of the exciting pump wave vector. Due to the symmetry group  $C_{3v}$  of the LN, the reduced nonlinear susceptibility tensor dictates the SPDC process through non-zero elements (i.e.,  $d_{15} = d_{31} = -4.88 \frac{\text{pm}}{\text{V}}$ ,  $d_{22} = 2.58 \frac{\text{pm}}{\text{V}}$  and  $d_{33} = -34 \frac{\text{pm}}{\text{V}}$  [42]). Therefore, the orientation of the far-field emission pattern along the z-axis can be attributed to the  $d_{33}$  component, which has the largest value compared to the other elements. Furthermore, the nonlinear emission in the opposite direction to the excitation propagation is due to the negative sign of this same component. The forward-to-backward ratios are 32% for the case of the glass above, i.e., the excitation laser coming directly from the side of the cube, meaning most emitted photons travel in a backward manner. When the cube was excited through the glass substrate, we obtained 35% forward emission, but most of the photon pairs are still emitted in backward direction (Fig. 3(D)). This implies a negligible effect from the glass substrate. Our system, therefore, is particularly interesting as it addresses the problem of directive SPDC emission. The understanding of

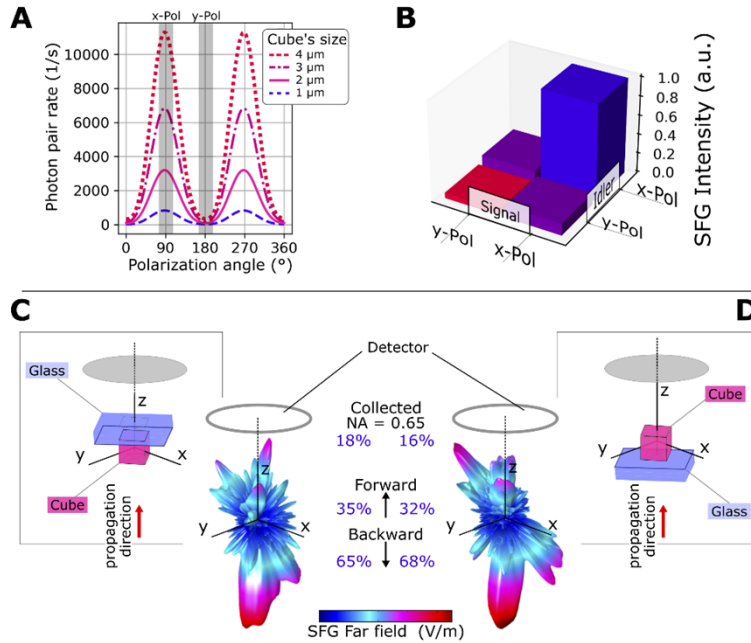


**Fig. 3.** (A) Simulation results show the input polarization dependence of the SPDC photon pair rate generated from LN microcubes with different sizes. The biphoton rate is proportional to the base area of the cube and maximal for the polarization angle of  $90^\circ/270^\circ$ , considering the case where the beam is polarized along the optical axis of the cube. (B) FEM simulation describe the intensity of SFG emission depending on the linear polarization of the signal and idler photons. The intensity is calculated for a microcube with the size of  $2 \mu\text{m}$  and is maximal for two photons linearly polarized along the optical axis of the microcube. (C-D) 3D schematics and far-field radiation profile of the SFG signal from a microcube with the size of  $2 \mu\text{m}$  for the two cases (C) the excitation wave propagates first through air, and the signal is collected on the glass side, and (D) the excitation wave propagates first through glass, and the SFG signal is collected on the airside. Comparatively slightly more SFG is produced in the forward direction as well as passes through a collection area ( $\text{NA} = 0.65$ ) for the first case.

radiation patterns can help to further optimize the setup to achieve a higher biphoton collection efficiency.

Finally, to consolidate our study, we performed measurements on various microcubes. Figures 4(A)-(C) present SEM images of three different cubes involved in the measurement with the corresponding sizes of  $2.5$ ,  $2.8$ , and  $3.6 \mu\text{m}$ , respectively. SPDC emission was indeed maximal when the pump polarization aligned along the optical axis of the cube (Fig. 4(D)-(F)).

Moreover, upon increasing the size of the cubes, we obtained improved photon pair rates from  $18$  to  $490 \text{ Hz}$  (photon pair rates of the 4 cubes are summarized in Table S1), respectively corresponding to cube 2 ( $2.5 \pm 0.1 \mu\text{m}$ ) and cube 4 ( $3.6 \pm 0.1 \mu\text{m}$ ). The lower biphoton rates of cube 2 and cube 3 probably stem from the internal morphological defects, which might suppress the nonlinear responses [46], however, the collection efficiency of the setup (see Supplementary, section 3) remains the main cause of much lower experimental values. We also determined the SPDC conversion efficiency for all cubes 1 to 4 by normalizing the photon pair rate over the cube volume and pump intensity. Those values are shown in Table S1, yielding a maximum conversion efficiency of  $20.6 \pm 2.5 \text{ GHz/Wm}$  obtained from cube 4, which is about an order of magnitude higher than the SPDC efficiency from AlGaAs nanoresonators [32], and three orders

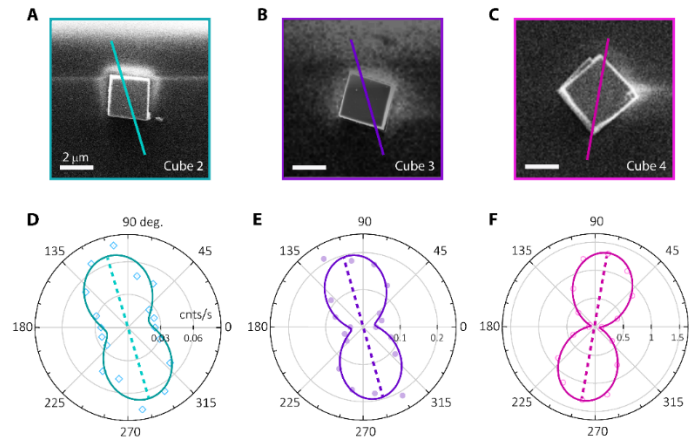


**Fig. 4.** SPDC measurements on different cubes. (A-C) SEM images of cubes 2, 3, and 4, respectively. (D-F) Bi-photon rate dependence on incoming pump polarization for different cubes, measured by extracting the photon pair generation rate while changing the pump polarization (see Supplementary, Fig. S7 for more detail on the measurements). The acquisition times are 30, 8, and 15 mins for cubes 2, 3, and 4, respectively. The optical axes (solid lines in Fig. 4(A)-(C)) and the polarization axes (dashed lines in Fig. 4(D)-(F)) serve as a guide to the eye.

of magnitude higher than the value achieved from typical nonlinear crystals [10]. This figure of merit demonstrates that our microcubes are a promising platform for the generation of photon pairs without the necessity of Mie-like resonances to support the SPDC process (Supplementary, Fig. S5).

### 3. Conclusions

In summary, we experimentally demonstrated photon pair generation via SPDC from LN microcubes. We obtained a maximum photon pair rate of  $490 \pm 60$  Hz from a  $3.6 \mu\text{m}$  cube, which implies a conversion efficiency of  $20.6 \pm 2.5$  GHz/Wm. Using FEM modeling, we presented the polarization correlation of the generated biphotons and their far-field emission profile. Our results demonstrate the capability of LN microcubes as an affordable and abundant nonclassical light source for flexible quantum-state engineering. Owing to the free-standing nature of the microcubes, they can be used as a versatile platform for integrated optical systems and free-space communications. Also, due to the relation between the geometry of these cubes and crystal structure, the optical axes of these cubes are easily detectable. Therefore, by rotating the pump polarizations along these axes, a maximum photon pair generation rate can be achieved. Further investigation on different geometries of the cubes obtained via controlling various parameters during the growth process might also boost the SPDC efficiency. Finally, the successful measurement of two-photon generation from a LN microcube via non-phase-matched SPDC opens the possibility to develop quantum networking with different frequency channels, and broadband tunable squeezed states for sensing applications.

**Funding.** Australian Research Council (DE180100070); Schweizerischer Nationalfonds zur Förderung der Wissenschaftlichen Forschung (Ambizione Grant No. 179966); European Research Council (714837); Schweizerischer Nationalfonds zur Förderung der Wissenschaftlichen Forschung (179099).

**Acknowledgments.** We thank Tomás Santiago-Cruz, Maria Chekhova, and Robert J. Chapman for fruitful discussions. We are thankful for the additional optical images taken by Helena Weigand and Olivier Jungo. We acknowledge the support of the Scientific Center for Optical and Electron Microscopy (ScopeM) of the Swiss Federal Institute of Technology (ETHZ). This work was also supported by the Swiss National Science Foundation Grant 179099,

the European Union's Horizon 2020 research and innovation program from the European Research Council under the Grant Agreement No. 714837 (Chi2-nano-oxides), Ambizione Grant No. 179966, and the Australian Research Council (grant number DE180100070).

**Disclosures.** The authors declare no conflicts of interest.

**Data availability.** Data underlying the results presented in this paper are not publicly available at this time but may be obtained from the authors upon reasonable request.

**Supplemental document.** See [Supplement 1](#) for supporting content.

## References

1. L. Caspani, C. Xiong, B. J. Eggleton, D. Bajoni, M. Liscidini, M. Galli, R. Morandotti, and D. J. Moss, "Integrated sources of photon quantum states based on nonlinear optics," *Light: Sci. Appl.* **6**(11), e17100 (2017).
2. Y. Wang, K. D. Jöns, and Z. Sun, "Integrated photon-pair sources with nonlinear optics," *Appl. Phys. Rev.* **8**(1), 011314 (2021).
3. J. L. O'Brien, A. Furusawa, and J. Vučković, "Photonic quantum technologies," *Nat. Photonics* **3**(12), 687–695 (2009).
4. D. E. Chang, V. Vuletić, and M. D. Lukin, "Quantum nonlinear optics - Photon by photon," *Nat. Photonics* **8**(9), 685–694 (2014).
5. L. Olislager, J. Safioui, S. Clemmen, K. P. Huy, W. Bogaerts, R. Baets, P. Emplit, and S. Massar, "Silicon-on-insulator integrated source of polarization-entangled photons," *Opt. Lett.* **38**(11), 1960 (2013).
6. J. E. Sharping, A. Coker, M. Fiorentino, P. Kumar, and R. S. Windeler, "Four-wave mixing in microstructure fiber," *Opt. Lett.* **26**(14), 1048 (2001).
7. C. K. Hong and L. Mandel, "Theory of parametric frequency down conversion of light," *Phys. Rev. A* **31**(4), 2409–2418 (1985).
8. K. Garay-Palmett, M. Corona, and A. U'Ren, "Spontaneous parametric processes in optical fibers: a comparison," *Rev. Mex. de Fis.* **57**, 3 (2013).
9. Y. H. Kim, S. P. Kulik, M. V. Chekhova, W. P. Grice, and Y. Shih, "Experimental entanglement concentration and universal Bell-state synthesizer," *Phys. Rev. A* **67**(1), 010301 (2003).
10. P. G. Kwiat, K. Mattle, H. Weinfurter, A. Zeilinger, A. V. Sergienko, and Y. Shih, "New high-intensity source of polarization-entangled photon pairs," *Phys. Rev. Lett.* **75**(24), 4337–4341 (1995).
11. W. Li and S. Zhao, "Generation of two-photon orbital-angular-momentum entanglement with a high degree of entanglement," *Appl. Phys. Lett.* **114**(4), 041105 (2019).
12. F. Kaneda, H. Suzuki, R. Shimizu, and K. Edamatsu, "Direct generation of frequency-bin entangled photons via two-period quasi-phase-matched parametric downconversion," *Opt. Express* **27**(2), 1416 (2019).
13. S. Castelletto, B. C. Johnson, V. Ivády, N. Stavrias, T. Umeda, A. Gali, and T. Ohshima, "A silicon carbide room-temperature single-photon source," *Nat. Mater.* **13**(2), 151–156 (2014).
14. I. Aharonovich and E. Neu, "Diamond nanophotonics," *Adv. Opt. Mater.* **2**(10), 911–928 (2014).
15. J. C. Loredó, N. A. Zakaria, N. Somaschi, C. Anton, L. de Santis, V. Giesz, T. Grange, M. A. Broome, O. Gazzano, G. Coppola, I. Sagnes, A. Lemaitre, A. Auffeves, P. Senellart, M. P. Almeida, and A. G. White, "Scalable performance in solid-state single-photon sources," *Optica* **3**(4), 433 (2016).
16. P. Tonndorf, R. Schmidt, R. Schneider, J. Kern, M. Buscema, G. A. Steele, A. Castellanos-Gomez, H. S. J. van der Zant, S. Michaelis de Vasconcellos, and R. Bratschkitsch, "Single-photon emission from localized excitons in an atomically thin semiconductor," *Optica* **2**(4), 347 (2015).
17. J. P. So, K. Y. Jeong, J. M. Lee, K. H. Kim, S. J. Lee, W. Huh, H. R. Kim, J. H. Choi, J. M. Kim, Y. S. Kim, C. H. Lee, S. Nam, and H. G. Park, "Polarization control of deterministic single-photon emitters in monolayer WSe<sub>2</sub>," *Nano Lett.* **21**(3), 1546–1554 (2021).
18. M. Toth and I. Aharonovich, "Single photon sources in atomically thin materials," *Annu. Rev. Phys. Chem.* **70**(1), 123–142 (2019).
19. T. T. Tran, K. Bray, M. J. Ford, M. Toth, and I. Aharonovich, "Quantum emission from hexagonal boron nitride monolayers," *Nat. Nanotechnol.* **11**(1), 37–41 (2016).
20. X. Guo, C. L. Zou, C. Schuck, H. Jung, R. Cheng, and H. X. Tang, "Parametric down-conversion photon-pair source on a nanophotonic chip," *Light: Sci. Appl.* **6**(5), e16249 (2017).
21. Y. Chen, M. Zopf, R. Keil, F. Ding, and O. G. Schmidt, "Highly-efficient extraction of entangled photons from quantum dots using a broadband optical antenna," *Nat. Commun.* **9**(1), 1–7 (2018).
22. S. J. U. White, N. M. H. Duong, A. S. Solntsev, J. H. Kim, M. Kianinia, and I. Aharonovich, "Optical repumping of resonantly excited quantum emitters in hexagonal boron nitride," *Phys. Rev. Appl.* **14**(4), 044017 (2020).
23. X. Cao, M. Zopf, and F. Ding, "Telecom wavelength single photon sources," *J. Semicond.* **40**(7), 071901 (2019).
24. S. Kurimura, Y. Kato, M. Maruyama, Y. Usui, and H. Nakajima, "Quasi-phase-matched adhered ridge waveguide in LiNbO<sub>3</sub>," *Appl. Phys. Lett.* **89**(19), 191123 (2006).
25. G. Fujii, N. Namekata, M. Motoya, S. Kurimura, and S. Inoue, "Bright narrowband source of photon pairs at optical telecommunication wavelengths using a type-II periodically poled lithium niobate waveguide," *Opt. Express* **15**(20), 12769 (2007).



26. R. Kou, S. Kurimura, K. Kikuchi, A. Terasaki, H. Nakajima, K. Kondou, and J. Ichikawa, "High-gain, wide-dynamic-range parametric interaction in Mg-doped LiNbO<sub>3</sub> quasi-phase-matched adhered ridge waveguide," *Opt. Express* **19**(12), 11867 (2011).
27. C. Wang, C. Langrock, A. Marandi, M. Jankowski, M. Zhang, B. Desiatov, M. M. Fejer, and M. Lončar, "Ultra-high-efficiency wavelength conversion in nanophotonic periodically poled lithium niobate waveguides," *Optica* **5**(11), 1438 (2018).
28. A. S. Solntsev and A. A. Sukhorukov, "Path-entangled photon sources on nonlinear chips," *Rev Phys.* **2**, 19–31 (2017).
29. C. Okoth, A. Cavanna, T. Santiago-Cruz, and M. V. Chekhova, "Microscale generation of entangled photons without momentum conservation," *Phys. Rev. Lett.* **123**(26), 263602 (2019).
30. T. Santiago-Cruz, V. Sultanov, H. Zhang, L. A. Krivitsky, and M. V. Chekhova, "Entangled photons from subwavelength nonlinear films," *Opt. Lett.* **46**(3), 653 (2021).
31. A. Nikolaeva, K. Frizyuk, N. Olekhno, A. Solntsev, and M. Petrov, "Directional emission of down-converted photons from a dielectric nanoresonator," *Phys. Rev. A* **103**(4), 043703 (2021).
32. G. Marino, A. S. Solntsev, L. Xu, V. F. Gili, L. Carletti, A. N. Poddubny, M. Rahmani, D. A. Smirnova, H. Chen, A. Lemaître, G. Zhang, A. V. Zayats, C. De Angelis, G. Leo, A. A. Sukhorukov, and D. N. Neshev, "Spontaneous photon-pair generation from a dielectric nanoantenna," *Optica* **6**(11), 1416 (2019).
33. T. Santiago-Cruz, A. Fedotova, V. Sultanov, M. A. Weissflog, D. Arslan, M. Younesi, T. Pertsch, I. Staude, F. Setzpfandt, and M. Chekhova, "Photon pairs from resonant metasurfaces," *Nano Lett.* **21**(10), 4423–4429 (2021).
34. M. Parry, A. Mazzanti, A. Poddubny, G. Della Valle, D. N. Neshev, and A. A. Sukhorukov, "Enhanced generation of nondegenerate photon pairs in nonlinear metasurfaces," *Adv. Photonics* **3**(05), 1–6 (2021).
35. S. Wang, C. Ji, P. Dai, L. Shen, and N. Bao, "The growth and characterization of six inch lithium niobate crystals with high homogeneity," *CrystEngComm* **22**(4), 794–801 (2020).
36. G. Poberaj, M. Koechlin, F. Sulser, A. Guarino, J. Hajfler, and P. Günter, "Ion-sliced lithium niobate thin films for active photonic devices," *Opt. Mater. (Amst)* **31**(7), 1054–1058 (2009).
37. A. S. Solntsev, P. Kumar, T. Pertsch, A. A. Sukhorukov, and F. Setzpfandt, "LiNbO<sub>3</sub> waveguides for integrated SPDC spectroscopy," *APL Photonics* **3**(2), 021301 (2018).
38. R. Geiss, S. Saravi, A. Sergeev, S. Diziain, F. Setzpfandt, F. Schrepel, R. Grange, E.-B. Kley, A. Tünnermann, and T. Pertsch, "Fabrication of nanoscale lithium niobate waveguides for second-harmonic generation," *Opt. Lett.* **40**(12), 2715 (2015).
39. F. Lacour, N. Courjal, M. P. Bernal, A. Sabac, C. Bainier, and M. Spajer, "Nanostructuring lithium niobate substrates by focused ion beam milling," *Opt. Mater. (Amst)* **27**(8), 1421–1425 (2005).
40. F. Timpu, J. Sendra, C. Renaut, L. Lang, M. Timofeeva, M. T. Buscaglia, V. Buscaglia, and R. Grange, "Lithium Niobate Nanocubes as Linear and Nonlinear Ultraviolet Mie Resonators," *ACS Photonics* **6**(2), 545–552 (2019).
41. O. A. Ivanova, T. S. Iskhakov, A. N. Penin, and M. V. Chekhova, "Multiphoton correlations in parametric down-conversion and their measurement in the pulsed regime," *Quantum Electron.* **36**(10), 951–956 (2006).
42. R. S. Weis and T. K. Gaylord, "Lithium niobate: Summary of physical properties and crystal structure," *Appl. Phys. A* **37**(4), 191–203 (1985).
43. A. N. Poddubny, I. V. Iorsh, and A. A. Sukhorukov, "Generation of photon-plasmon quantum states in nonlinear hyperbolic metamaterials," *Phys. Rev. Lett.* **117**(12), 123901 (2016).
44. F. Lenzini, A. N. Poddubny, J. Titchener, P. Fisher, A. Boes, S. Kasture, B. Haylock, M. Villa, A. Mitchell, A. S. Solntsev, A. A. Sukhorukov, and M. Lobino, "Direct characterization of a nonlinear photonic circuit's wave function with laser light," *Light: Sci. Appl.* **7**(1), 17143 (2018).
45. J. S. Müller, A. Morandi, R. Grange, and R. Savo, "Modeling of random quasi-phase-matching in birefringent disordered media," *Phys. Rev. Appl.* **15**(6), 064070 (2021).
46. Y. Furukawa, K. Kitamura, S. Takekawa, K. Niwa, and H. Hatano, "Stoichiometric Mg:LiNbO<sub>3</sub> as an effective material for nonlinear optics," *Opt. Lett.* **23**(24), 1892 (1998).